4FNF DOUBLY EXCITED AUTOIONIZING SERIES IN BARIUM

de Graaff, R.J.; Ubachs, W.M.G.; Hogervorst, W.

published in
Physical Review A. Atomic, Molecular and Optical Physics
1992

DOI (link to publisher)
10.1103/PhysRevA.45.166

document version
Publisher's PDF, also known as Version of record

$4fnf$ doubly excited autoionizing series in barium

R. J. de Graaff, W. Ubachs, and W. Hogervorst
Laser Centre Free University Amsterdam, Faculteit Natuurkunde en Sterrenkunde, De Boelelaan 1081, 1081 HV Amsterdam, The Netherlands
(Received 17 July 1991)

In a two-step pulsed-laser atomic-beam experiment we have studied doubly exicted $4fnf$ series of barium with energy of ~ 11 eV above the atomic ground state ($6s^2$) and 6 eV above the first ionization limit ($6s$). Starting from $5d^2\,{}^3F_3$, ${}^1G_4$ metastable states, $4f_{5/2}n'f$ $J=2-6$ ($9 \leq n' \leq 46$) states and $4f_{7/2}n''f$ $J=3-6$ ($n''=19$, 20, 21, 25, and 40) states were excited using intermediate $5dnf$ autoionizing Rydberg states. The $4f_{5/2}n'f$ $J=2-6$ states strongly interact with $4f_{7/2}n''f$ $J=2-6$ ($8 \leq n'' \leq 20$) and $7pn'''f$ $J=2-5$ ($6 \leq n''' \leq 10$) states. The excitation spectra were analyzed and interpreted using multichannel quantum-defect theory as well as a limited Slater-Condon analysis. The quantum defects of the $4fnf$ series are large (0.5–1.4), which is an indication for considerable two-electron correlation effects.

PACS number(s): 32.80.Dz, 32.30.−r

I. INTRODUCTION

Multistep and multiphoton excitation techniques have been successfully applied in the study of the properties of highly excited atomic states. In particular, much attention has been given to atoms with two valence electrons such as the alkaline-earth metals. Results on their doubly excited autoionizing states have been reported over the last few years by several groups [1–6]. These investigations are of interest as they can provide information on correlation effects between electrons in excited atomic states. Commonly, one of the two valence electrons is first promoted from the ground state to a high Rydberg state nl (n is the principal quantum number, and l is the orbital angular momentum) followed by the (stepwise) excitation of the second electron, resulting in $Nl'n'l$ states ($n' \sim n$ and $N < n'$). Barium is the most convenient atom for these studies as its high-lying doubly excited states converging to the Ba^{2+} limit have the lowest energies among the alkaline-earth metals and are accessible with a few laser-excitation steps. It is this element in which the highest principal quantum number N of the inner electron has been reached [4,5,7]. In all investigations thus far, except those of the $4fng$ series of barium [7], at least one of the electrons penetrated the xenon-core-electron cloud deeply (l or $l' < 3$). In the case of core-penetrating electrons, the effects of electron correlations are relatively small, and for $l \sim l'$, autoionization decay rates are large.

In this paper we present results on an investigation of the $4fnf$ autoionizing series of barium. The $4fnf$ series converge to the $4f_{5/2}$ and $4f_{7/2}$ thresholds at 90 293.49 and 90 518.19 cm^{-1}, respectively, i.e., $\sim 50\,000$ cm^{-1} above the first ionization limit ($6s$ limit at 42 034.902 cm^{-1}). Our experiment differs in an important aspect from others in that we do not use the $6s^2\,{}^1S_0$ ground state in the excitation process, but metastable states of the $5d^2$ configuration (for this experiment $5d^2\,{}^1G_4$ and ${}^3F_3$). Then only two excitation steps via $5dnf$ $J=3-5$ intermediate states are required to reach $4fnf$ $J=2-6$ states. This scheme facilitates the J-value assignment of the final states because well-defined J values for the intermediate states can be selected. The present investigation is a continuation of our earlier work on doubly excited autoionizing series of the $5dnf$, $6pnp$, $6pnf$, and $6pnh$ configurations [3,8–11]. In particular, the detailed knowledge on the $5dnf$ configuration turned out to be of importance for the interpretation of our data on the $4fnf$ series, as will be shown.

The $4fnf$ configuration is of special interest as both electrons move to a large extent outside the core-electron cloud and have the same orbital angular momentum. The Ba^{2+} potential for the f electron shows two minima. This is a consequence of the action of both the Coulomb and centrifugal potential [12,13]. In Ba^+ the nf wave functions are partially collapsed and localized in both minima of the potential. This is reflected in large phase shifts of the radial wave functions and consequently large quantum defects (~ 0.9) of the nf states in the ion compared to quantum defects of nf states in, e.g., Cs or Ca^+ (< 0.1) [14]. For the $4f$ states (quantum defect ~ 0.3), the penetration into the inner valley appears to be less pronounced [13]. In $Nlnf$ states of barium with $l \leq 2$, the inner Nl electron partly screens the 2^+ charge for the nf electron. As a consequence, these series have much smaller quantum defects compared to the nf series in Ba^+ (for $6snf$ and $5dnf \sim 0.1$ and for $6pnf \sim 0.3$). This screening is less effective in $Nfnf$ states. Therefore, these states will be extremely sensitive to electron-correlation effects which strongly influence this screening [15]. Of interest are changes in both quantum defect and linewidth as a function of N and n. Especially attractive will be the excitation and localization of the $4f^2$ multiplet, in which the direct and exchange electrostatic interactions are identical. Furthermore, $4f$ states have almost circular orbits ($l=n-1$) and several members of the $4f^2$ multiplet might be so-called Wannier states [16,17]. In the present work, in which these states could not be detected, results on the $4fnf$ $J=2-6$ series in the

range of $n=8-46$ are reported.

The paper is organized as follows. In Sec. II we will give details of the experiment and present experimental results. In Sec. III the data will be interpreted and analyzed, whereas in Sec. IV a limited Slater-Condon parametrization of the $4fnf$ configuration will be presented. Finally, in Sec. V some conclusions will be given.

II. EXPERIMENTAL RESULTS

The experimental setup to excite the $4fnf$ series from metastable states of the $5d^2$ configuration is similar to the one used in earlier work on, e.g., the $6pnl$ series in barium [3,10]. An atomic beam was produced by heating a tantalum oven to a temperature of about 1000 K. In between the heating filament and oven orifice, a low-voltage discharge was maintained to populate the metastable states. The atomic beam was intersected perpendicularly by the light of two tunable lasers to excite the $4fn'f$ states via the intermediate $5dnf$ autoionizing states. The excitation scheme is shown in Fig. 1. The $5dnf$ intermediate states were excited with a pulsed narrow-band dye laser (Quanta Ray PDL3, bandwidth 0.07 cm^{-1}) using Coumarine or Exalite dyes from the $5d^2\,{}^1G_4$ (at 24 696.278 cm^{-1}) and $5d^2\,{}^3F_3$ (at 21 250.173 cm^{-1}) metastable states, respectively. This dye laser was pumped with 30% of the 355-nm light from a Nd:YAG (YAG denotes yttrium aluminum garnet) laser (Quanta Ray GCR4). A few hundred μJ were used for the first excitation step. The remaining 70% of the pump light was used to pump a second Coumarine 460 dye laser (Quanta Ray PDL2, bandwidth 0.3 cm^{-1}). The blue light of this laser was frequency doubled in a β-barium borate (BBO) crystal for the excitation of the $4fn'f$ states from $5dnf$ states. This transition required laser light with a wavelength close to the $5d$-$4f$ ionic transition ($\sim$230 nm). In the second excitation step only a few μJ of laser energy were used, which was sufficiently low to avoid depletion saturation. The two laser beams were spatially overlapped in the interaction region with the atomic beam, and care was taken to have a homogeneous power distribution. We used linear polarizations for the laser beams as no significant effect of laser polarization will result in excitation from $J=3$ and 4 initial states. The lifetimes of the intermediate $5dnf$ states, varying from 20 ns (around $5d_{3/2}40f$) to a few picoseconds ($5d_{5/2}nf$ states with low n), influence the number of atoms available for further excitation. The 5-ns laser pulses were carefully overlapped in time as well to optimize population of the $4fnf$ states. A home-built echelle-grating wavelength meter (accuracy 0.2 cm^{-1}) was used for calibration.

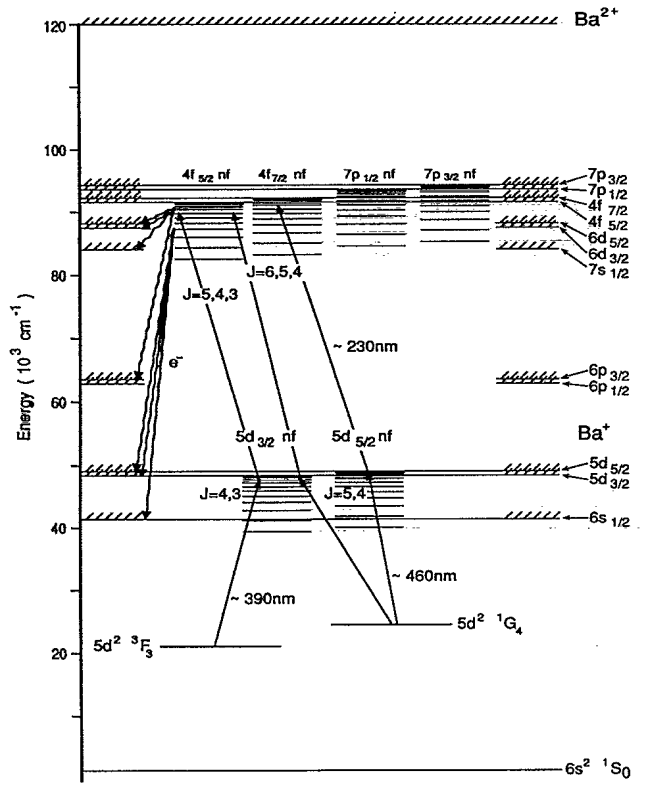

FIG. 1. Energy-level diagram of barium and the excitation scheme.

We detected the electrons from the autoionization of $4fnf$ states with an electron multiplier. A complication was that 230-nm light produces large Ba^+ and 2-eV electron-background signal by direct photoionization of metastable states in the beam. Therefore, only electrons with an energy larger than 2 eV were detected. This was accomplished with two spherical grids (transmission $>75\%$) serving as electrostatic lenses between the field-free detection region and electron multiplier. A variable repulsive voltage was applied, also enabling the measurement of electron-energy spectra with a resolution of 0.2 eV. Signals were stored in a VME-10 computer. We applied signal averaging over 12 shots per wavelength setting. The $6d\epsilon l$, $5d\epsilon l$ ($5d$ limits at $\sim$47 000 cm^{-1}), and $6p\epsilon l$ continua ($6p$ limits at $\sim$63 000 cm^{-1}) are the most important decay channels for the series under investigation. A consequence of our detection scheme was that the low-energy electrons (<2 eV) resulting from autoionization into $6d\epsilon l$ continua ($6d$ limits at $\sim$88 000 cm^{-1}) could not be observed.

In the first excitation step ($5d^2$ $J=3,4$ to $5dnf$ $J=3,4,5$) we used the narrowest-bandwidth dye laser to resolve the different J states of the $5dnf$ multiplet to the highest n value possible. This ensures maximum selectivity in the next excitation step to $4fn'f$ $J=2-6$ states. From $5d^2\,{}^1G_4$ we selectively excited the single $J=5$ and the two $J=4$ $5d_{3/2}nf$ states up to $n=34$ with a few exceptions where the $5d_{3/2}nf$ series are perturbed by members of the $5d_{5/2}nf$ and/or $5d_{5/2}np$ series [9]. Also, $5d_{5/2}nf$ $J=4$ states for $n=17,20,21,25,40$ and the $5d_{5/2}25f$ $J=5$ level were excited from $5d^2\,{}^1G_4$. Because of the relatively short lifetime of the $5d_{5/2}nf$ intermediate states, only a limited set of data could be taken. To add information we also used the $5d^2\,{}^3F_3$ metastable state to excite $5d_{3/2}nf$ $J=3$ and 4 states. Only in a few cases ($n=20$, 21, 23, and 25) did we succeed to excite further from the $5d_{3/2}nf$ $J=3$ levels as a result of their relatively short lifetimes. $\Delta J=-1$ transitions from $5d^2$ metastable

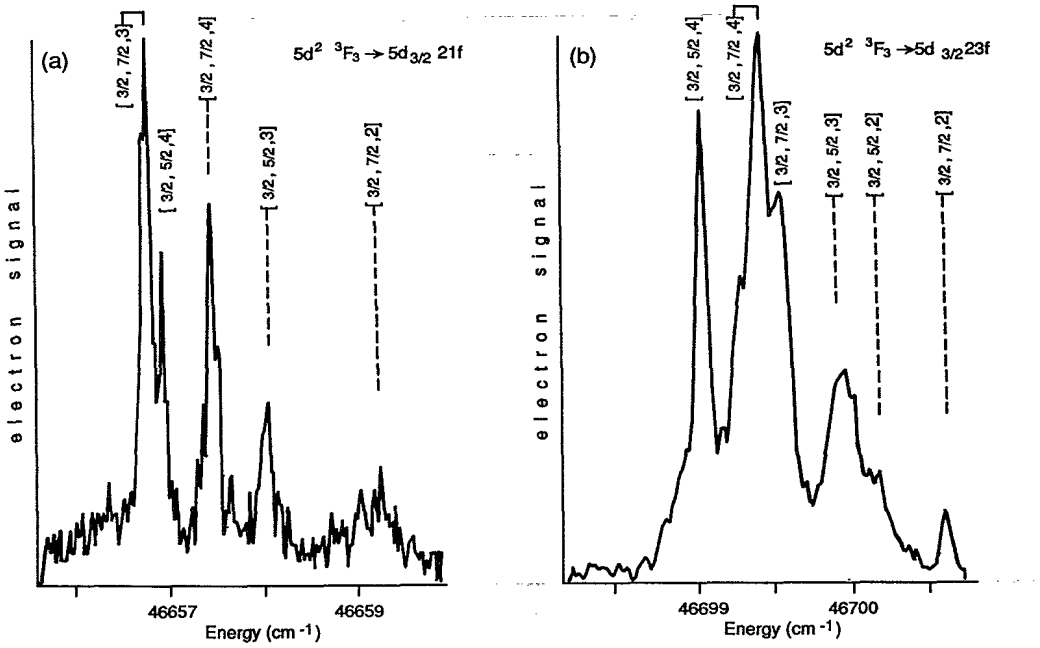

FIG. 2. Spectra of $5d_{3/2}nf\ J=4,3,2$ autoionizing states near $5d_{5/2}np$ perturbers as recorded in excitation from the $5d^2\,^3F_3$ intermediate state: (a) $n=21$ and (b) $n=23$. $5d_{3/2}nf$ states are labeled according to $[j_1,j_2,J]$.

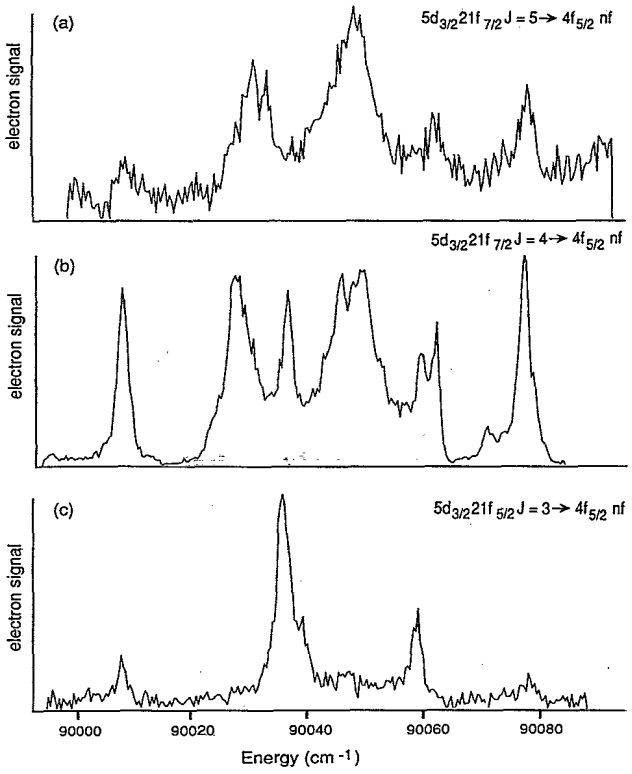

FIG. 3. Spectra of $4f_{5/2}n'f\ J=6,5,4,3$ states as recorded in excitation from $5d_{3/2}21f\ J=5,4,3$ [see Fig. 2(a)]. Assignments are included in Fig. 10(a). (a) Excitation from $5d_{3/2}21f_{7/2}\ J=5$, (b) excitation from $5d_{3/2}21f_{7/2}\ J=4$, and (c) excitation from $5d_{3/2}21f_{5/2}\ J=3$.

states to $5d_{3/2}nf$ states have low probability. However, $5d_{3/2}nf\ J=3,2$ states can be perturbed by $5d_{5/2}np$ states, which will result in an increased oscillator strength for the excitation of $J=2$ states from $5d^2\,^3F_3$ and $J=3$ from $5d^2\,^1G_4$. Indeed, $5d_{3/2}nf\ J=2$ resonances were observed for $n=21$–23 (see Fig. 2). Although we were able to detect $5d_{3/2}nf\ J=3$ from $5d^2\,^3F_2$ (at 20 934.013 cm^{-1}) as well, low signal strengths prohibited further use of this metastable state.

Examples of various spectra recorded are given in Figs. 2–6 and 7(a). In Fig. 2, spectra of the excitation $5d^2\,^3F_3 \rightarrow 5d_{3/2}nf\ J=2,3,4$ for $n=21$ and 23 are shown. It illustrates that many of the $5d_{3/2}nf\ J$ states can be used for selective further excitation. The use of various intermediate $5d_{3/2}nf\ J$ states provides a wealth of information on the final $4fnf$ states. This is illustrated in Figs. 3 and 4 where spectra of the $4f_{5/2}n'f\ J=2$–6 configuration excited from the various $5d_{3/2}21f\ J=3$–5 and $5d_{3/2}20f\ J=3,4$ states are reproduced. In the excitation spectrum from the $5d_{3/2}15f\ J=5$ intermediate state, a sharp resonance was observed, as shown in Fig. 5. This resonance, using the Slater-Condon analysis discussed in Sec. IV, is identified as a mixture of $4f_{5/2}16f_{7/2}$ and $4f_{7/2}13f_{5/2}\ J=6$ states and appears to have the laser linewidth. In Fig. 6 a spectrum taken from the $5d_{5/2}20f\ J=4$ intermediate state is plotted. Figure 7(a) shows an excitation spectrum from the (unresolved) $5d_{3/2}40f\ J=5,4,3$ states. Moderate uv power ($\sim$0.5 mJ) was used to obtain this "shake-up–shake-down" spectrum (see Sec. III B). The identification of the resonances in the spectra and analysis of the data are complicated. This is the subject of the next section.

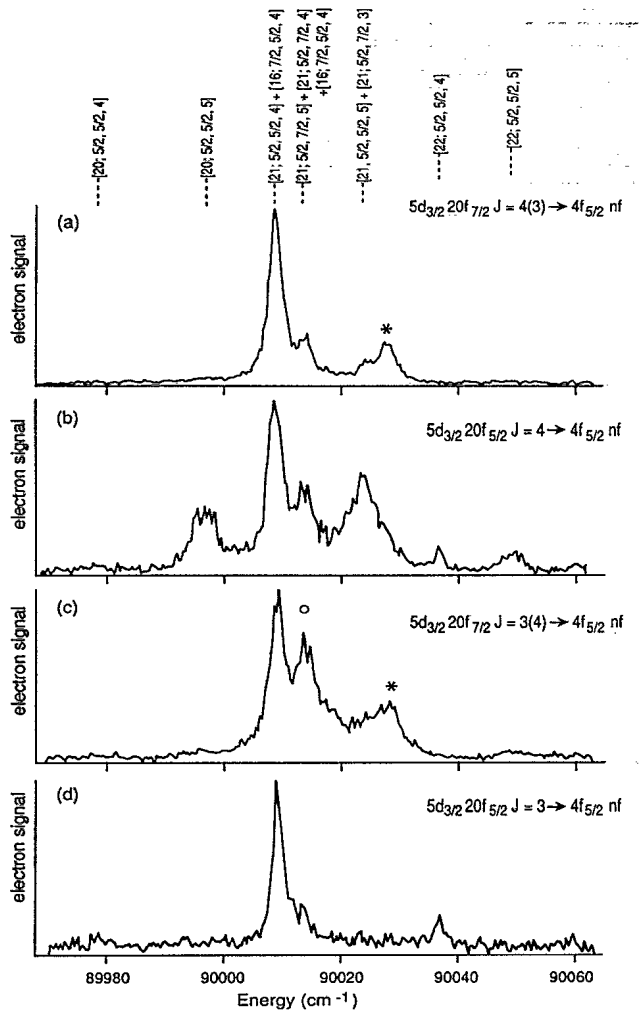

FIG. 4. Spectra of $4f_{5/2}n'f$ $J=5,4,3$ states as recorded in excitation from $5d_{3/2}20f_{5/2,7/2}$ $J=4,3$. (a) Excitation from $5d_{3/2}20f_{7/2}$ $J=4$, which is almost coincident with $5d_{3/2}20f_{7/2}$ $J=3$; (b) excitation from $5d_{3/2}20f_{5/2}$ $J=4$; (c) excitation from $5d_{3/2}20f_{7/2}$ $J=3$; and (d) excitation from $5d_{3/2}20f_{5/2}$ $J=3$. The resonances marked with an asterisk were not identified, and the assignment of the peak marked with an open circle is uncertain. $4fnf$ states are labeled according to $[n;j_1,j_2,J]$.

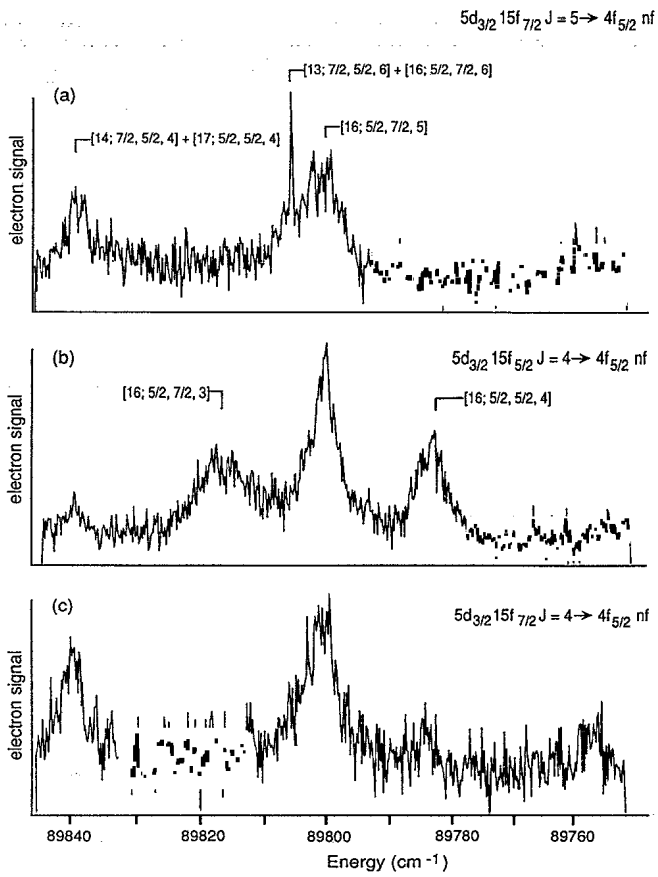

FIG. 5. Spectrum of the $4f_{5/2}n'f$ $J=6,5,4$ series as recorded in excitation from the $5d_{3/2}15f$ $J=5$ state. $4fnf$ states are labeled according to $[n;j_1,j_2,J]$. Note the narrow $J=6$ resonance, which has a dominant $4f_{7/2}n''f$ character.

III. INTERPRETATION AND ANALYSIS

A. 5dnf intermediate states

The interpretation and analysis of the $4fn'f$ spectra requires detailed knowledge of the various intermediate $5dnf$ series involved as well as of their perturbations. Therefore, we first summarize the information pertaining to this $5dnf$ configuration.

Eight $5d_{3/2}nf$ series (one series each for $J=1$ and 5 and two series for each value $J=2$–4) exist, converging to the $5d_{3/2}$ limit at 46 908.752 cm^{-1}, and 12 $5d_{5/2}nf$ series (one series each for $J=0$ and 6 and two series for each value $J=1$–5) to the $5d_{5/2}$ limit at 47 709.726 cm^{-1}. Series with the same J value mutually interact. In addition, the $5d_{3/2}nf$ series with $J\leq 4$ are perturbed by members of the $5d_{5/2}np$ configuration. The $5d_{5/2}nf$ $J=6,0$ series have not been observed thus far. The $5d_{3/2}nf$ and $5d_{5/2}nf$ $J=5,4$ series were studied by Bente and Hogervorst [9] in pulsed- and cw-laser experiments. The narrow linewidths of many of these $5d_{3/2}nf$ states allowed for hyperfine-structure measurements [8], providing detailed information on the wave functions of $J=4$ states as well as indications for a perturbation in the $J=3$ series. These experiments and their detailed multichannel quantum-defect analyses mapped out the interactions of the $5d_{3/2}nf$ $J=5,4$ series with members of the $5d_{5/2}nf$ $J=5,4$ configurations and, for $J=4$, with $5d_{5/2}np$ $J=4$ states. Less detailed information is available on the $5dnf$ $J=3$ series. These series were investigated in a pulsed-laser experiment by Jones [18], and some of his results were reproduced in our experiment (see, e.g., Fig. 2). In general, the $5d_{3/2}nf$ series are perturbed by $5d_{5/2}n'f$ states ($n'=9$–11) near $n=11$, 14, 19, and 31 and for $J\leq 4$ by $5d_{5/2}n''p$ states ($n''=13$–15) near $n=15$, 21, and 38–41. To our knowledge, $5d_{3/2}nf$ $J=2$ states were not observed before. The presence of $5d_{3/2}nf$ $J=2$ resonances in Fig. 2 is unexpected as, in general, $\Delta J=-1$ transitions are weak in excitation of $5dnf$ from $5d^2$ states. The oscillator strength for excitation of these series in between $n=21$–23 is enhanced by

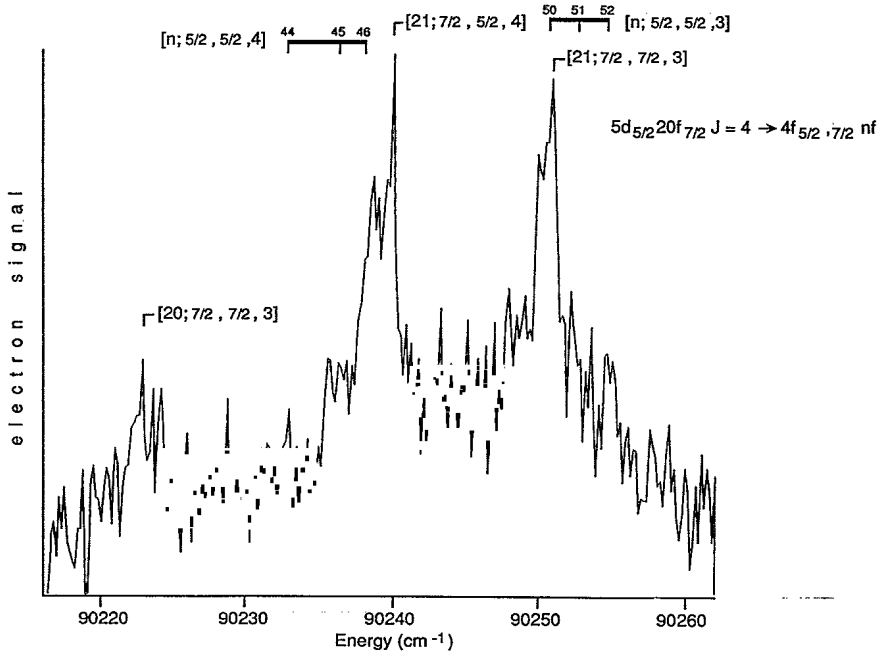

FIG. 6. Spectrum of the $4f_{5/2,7/2}n'f$ $J=6,5,4$ series as recorded in excitation from the $5d_{5/2}20f_{7/2}$ $J=4$ state. $4fnf$ states are labeled according to $[n;j_1,j_2,J]$.

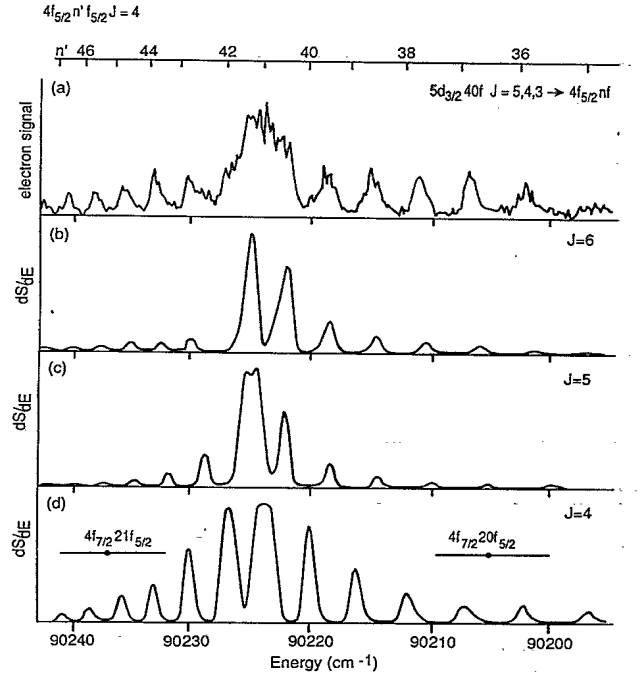

FIG. 7. Experimental "shake-up–shake-down" $4f_{5/2}n'f$ spectrum from $5d_{3/2}40f_{7/2}$ $J=4$ as well as calculated $4f_{5/2}n'f$ $J=6,5,4$ resonances using MQDT parameters from Tables II–V. (a) Spectrum from excitation out of the $5d_{3/2}40f_{7/2}$ $J=4$ intermediate state (fitted positions of $4f_{5/2}n'f_{5/2}$ $J=4$ states are included for convenience, (b) calculation for $J=6$, (c) calculation for $J=5$, and (d) calculation for $J=4$. Local enhancement of the $4f_{5/2}n'f_{5/2}$ $J=4$ detection efficiency by $4f_{7/2}n''f_{5/2}$ $J=4$ perturber character is clearly visible.

the $5d_{5/2}14p$ perturbing character. In excitation of $5dnp$ from $5d^2$ states, $\Delta J=-1$ is favored. The $5dnf$ $J=1$ series has been studied recently in detail in pulsed-laser experiments [19,20].

The data on the $5dnf$ multiplet were used in a Slater-Condon analysis of the configuration in terms of direct and exchange electrostatic interactions [21]. It provided wave functions for the various fine-structure states of the multiplet in energy regions were perturbers are absent. The quality of this fit is illustrated by the fact that the wave functions obtained for the $5d_{3/2}nf$ $J=4$ states are in excellent agreement with those deduced from hyperfine-structure measurements [8]. We used our analysis to characterize unperturbed $5d_{3/2}nf$ $J=3$ states. The Slater-Condon analysis indicates that, in the unperturbed multiplet, the $5d_{3/2}nf_{7/2}$ $J=4$ states lie close in energy to $5d_{3/2}nf_{7/2}$ $J=3$ and, within the laser linewidth, coincide with $5d_{3/2}nf_{5/2}$ $J=2$ states for $n>15$. This analysis is not well suited to reproduce the positions of the perturbed $J=2$ levels for $n=21$–23 in Fig. 2.

B. $4fnf$ configuration: General

The $4fnf$ configuration has 12 $4f_{5/2}nf$ series (one series each for $J=0$ and 6 and two series for each value $J=1$–5) converging to the $4f_{5/2}$ limit at 90 293.49 cm^{-1} and 14 $4f_{7/2}nf$ series (one series each for $J=0$ and 7 and two series for each value $J=1$–6) converging to the $4f_{7/2}$ limit at 90 518.19 cm^{-1}. From the intermediate $5d_{3/2}nf$ $J=5,4,3$ states, using the isolated core-excitation (ICE) method [22], we excited $4f_{5/2}n'f$ states with $J=6$–2.

Similarly both $4f_{5/2}n'f$ and $4f_{7/2}n''f$ $J=6-3$ states were populated from $5d_{5/2}nf$ $J=5,4$ intermediate states, but because of a much shorter lifetime of the latter states, only a limited set of data was recorded. The $4f_{7/2}n'f$ states interact with the $4f_{5/2}nf$ series. As the fine-structure splitting of the $4f$ ionic state is small (~ 225 cm^{-1}), many $4f_{5/2}nf$ states will be strongly mixed with $4f_{7/2}n'f$ states, which hampers assignment. Furthermore, 6 eV above the first ionization limit, a multitude of interacting series exists. Most important for the $4fnf$ configuration is interaction with $7pn''f$ series converging to the $7p_{1/2}$ limit at 91 424.95 cm^{-1} (four series, one series each for $J=2$ and 4 and two series for $J=3$) and to the $7p_{3/2}$ limit at 92 046.12 cm^{-1} (eight series, one series each for $J=1$ and 5 and two series for each value $J=2-4$). Quantum defects of $mlnl'$ ($l,l'\leq 2$) series are found to be linearly dependent upon m with a coefficient $\beta\sim 0.3$ [4,23]. As $6pnf$ series have quantum defects of ~ 0.2 [10], this relation predicts quantum defects of ~ 0.5 for $7pnf$ series, although at low n energy dependencies are expected. Consequently, $7p_{1/2}n''f$ states with $n''=7-10$ may perturb $4f_{5/2}nf$ series near $n=9,12,17,36$ and $7p_{3/2}n''f$ states with $n''=6-8$ near $n=8,11,24$. The $4f_{7/2}nf$ series may be perturbed around $n=8,10,13,19,36$ by $7p_{1/2}n''f$ states with $n''=7-11$ and around $n=7,10,16$ by $7p_{3/2}n''f$ states with $n''=7-9$.

The $4fnf$ series autoionize into several continua. For $4f_{5/2}nf$ series, $6d\epsilon l$, $5d\epsilon l$, $6p\epsilon l$, $7s\epsilon l$, and $6s\epsilon l$ continua are available. Decay into $ms\epsilon l$ continua is unlikely because of the large change of angular momentum involved in such a process. For $4f_{7/2}nf$ states above the $4f_{5/2}$ limit also, the $4f_{5/2}\epsilon l$ continuum is available. As only electrons with energies larger than 2 eV were detected, decay into the $6d\epsilon l$, $7s\epsilon l$, and $4f_{5/2}\epsilon l$ channels was not observed. This implies that comparing relative oscillator strengths when exciting several $4fn'f$ final states from one specific $5dnf$ intermediate state has only limited value as the different $4fn'f$ J states may all have different branching ratios. For the same reason it is also not feasible to deduce values for the oscillator strengths. Selection rules ($\Delta J=0,\pm 1$) and calculated oscillator-strength distributions are, however, important tools to interpret the observed spectra. For example, calculations based upon jj- or jK-coupled $4fnf$ wave functions show that in case of excitation from $5d_{3/2}nf_{5/2}$ $J=3$ states the spectrum will contain doublets of $4f_{5/2}nf$ resonances. The transition to $4f_{5/2}n'f_{5/2}$ $J=4$ (or $4f_{5/2}n'f[9/2]$ $J=4$) has largest intensity ($\Delta J=+1$), whereas the transition to $4f_{5/2}n'f_{5/2}$ $J=3$ (or $4f_{5/2}n'f[7/2]$) will be a factor of 2 weaker ($\Delta J=0$). Excitation from $5d_{3/2}nf_{7/2}$ $J=3$ gives a similar spectrum in which mainly $4f_{5/2}n'f_{7/2}$ $J=4$ (or $4f_{5/2}n'f[7/2]$ $J=4$) and $4f_{5/2}n'f_{7/2}$ $J=3$ (or $4f_{5/2}n'f[9/2]$) are involved. The $\Delta J=-1$ transitions are at least a factor of 10 less probable. When $5d_{3/2}nf$ $J=4$ intermediate states are used, the correct compositions of these states must be used to calculate oscillator strengths as they are not well described in either jj or jK coupling [8,9]. This will result in the appearance of a third (a second $\Delta J=+1$) or even fourth peak (a second $\Delta J=0$). Again, the calculated oscillator strengths are small for $\Delta J=-1$ transitions. The identification of resonances in the $4fn'f$ spectra is further complicated by the overlap in energy of intermediate $5d_{3/2}nf$ states with different J values, in several cases induced also by interaction with $5d_{5/2}n''l$ perturbing states.

However, observed relative intensities of specific final states excited from different $5dnf$ intermediate states were of use in the assignment. Helpful in the identification was that the $4fnf$ $J=6$ series is not perturbed by $7pn'f$ states. The $J=5$ series may be perturbed by a single $7p_{1/2}n'f$ and two $7p_{3/2}n'f$ series. The $4fnf$ series with $J=4-2$ may each be interacting with four $7pn'f$ series. Branching ratios in the autoionization process are sensitive to the perturber character mixed into the wave functions of $4f_{5/2}nf$ states. Therefore, it is possible to observe the presence of a perturber state even if this state seems to have little effect on the energy positions of the $4fnf$ states. Extra information used to assign observed features to specific series was obtained from measurements of electron energies (larger than 2 eV), thus resolving several of the autoionization routes of the states involved.

Energies of strong resonances were graphically related to series in Lu-Fano plots. The energies were deconvoluted for the "sinc-overlap function" (see hereafter) by averaging energy positions of specific resonances excited from $5dnf$ intermediate states with different n values. In Lu-Fano plots, strong interactions show on first sight. This is illustrated in Figs. 8 and 9. Figure 8 shows two perturbed $4f_{5/2}nf$ $J=5$ series with reduced eigenquantum defects of 0.1 and 0.8. The series with quantum defect 0.1 strongly interacts with $7p_{3/2}8f_{7/2}$ $J=5$, whereas the series with defect 0.8 interacts with $4f_{7/2}nf$ states. In Fig. 9, $4f_{5/2}nf$ $J=6$ states are plotted. These states interact with states belonging to one of the two $4f_{7/2}n'f$ $J=6$ series. J values were tentatively assigned to the different series. Next, we performed multichannel quantum-defect theory (MQDT) analyses for each J value. Observed spectra were reproduced by summing

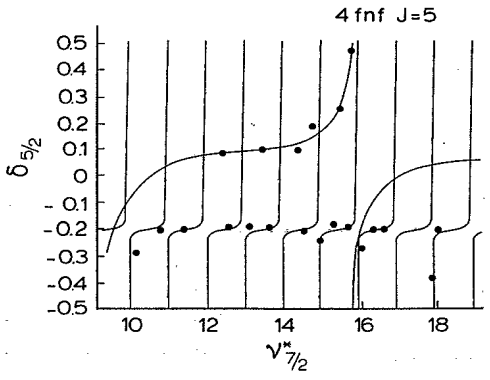

FIG. 8. Lu-Fano plot of the strongest $4f_{5/2}n'f$ $J=5$ resonances. The energy positions as observed from several $5d_{3/2}nf$ J intermediate states were averaged to minimize effects of the sinc function. The plot shows evidence of a strong interaction of the $4f_{5/2}n'f$ $J=5$ series with quantum defect 1.1 with $7p_{3/2}8f$ $J=5$.

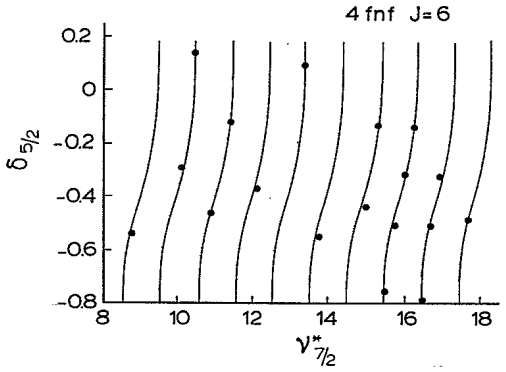

FIG. 9. Lu-Fano plot of the strongest $4f_{5/2}n'f$ $J=6$ resonances. Note the strong interaction between the $4f_{5/2}n'f$ $J=6$ series and one of the two $4f_{7/2}n''f$ $J=6$ series.

calculated spectra for all J. The curves drawn in Figs. 8 and 9 are based upon the final MQDT parameters, excluding continuum interactions.

We used the MQDT formalism of Cooke and Cromer, which is extensively discussed elsewhere and is especially adapted to describe ICE spectra [24,25]. Experimental data are parametrized in terms of quantum defects δ_i, interaction parameters R_{ij}, and dipole moments D_α of channels (bound series with corresponding continua). The quantum defect represents the phase shift in the wave function of the outer electron when it scatters at the inner valence or core electrons. We included linear energy dependencies of these quantum defects relative to the $4f_{7/2}$ limit whenever necessary. The interaction parameters are scattering matrix elements, describing intraconfiguration mixing of "collision" channels as well as configuration interactions. In the calculation of the oscillator-strength distribution dS/dE, the parametrized dipole moments D_α are used. They represent the excitation probability of phase-shifted channels in the ICE approximation [24]. The probability of the outer electron to be "shaken" into an orbit with different n during the excitation process $\langle nf|n'f\rangle$ is described by the well-known "shake-up–shake-down" function $\delta_{l,l'}\mathrm{sinc}[\pi(\nu-\nu')]$ [26]. Here ν and ν' are the effective principal quantum numbers for initial and final states, respectively. This sinc term leads to low excitation probability of perturbing states. This is due to the fact that the ν' of perturbing states usually differs significantly from ν. It explains that $4fnf$ series with the same reduced quantum defect as the intermediate states (~ 0.1) are only excited at $\nu=\nu'$. In the MQDT analyses of the various series presented in this report, the number of available continua was larger than the number of bound channels. Such systems can be presented by n channels interacting with n appropriately chosen continua [25]. Therefore, the number of continuum channels was set equal to the number of closed channels. No interference effects related to interaction of more than one closed channel with a specific continuum were observed in the spectra. In this MQDT model it is difficult to correct for the fact that the $6d\epsilon l$ decay channel was not detected. Examples of calculated spectra are included in Figs. 7 and 10. Figures

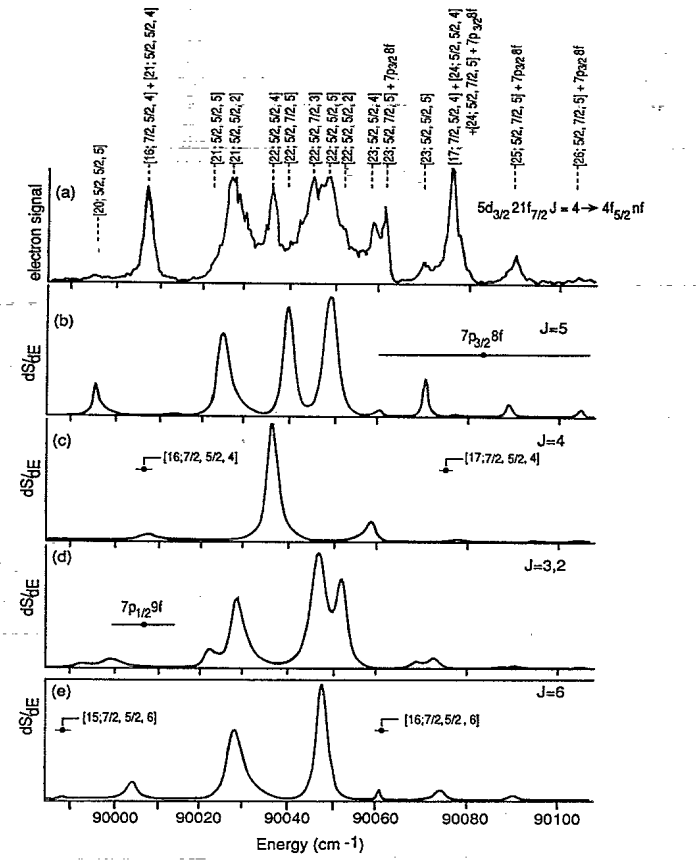

FIG. 10. Calculated $4f_{5/2}n'f$ $J=6,5,4,3$ spectra, using MQDT parameters from Tables II–V. (a) Experimental spectrum from the excitation out of the $5d_{3/2}21f_{7/2}$ $J=4$ intermediate state, (b) calculation for $J=5$, (c) calculation for $J=4$, (d) calculation for $J=3$, and (e) calculation for $J=6$ (not excited from $5d_{3/2}21f_{7/2}$ $J=4$). $4fnf$ states are labeled according to $[n;j_1,j_2,J]$. Local enhancement of the $4f_{5/2}n'f_{5/2}$ $J=4$ detection efficiency by $4f_{7/2}n''f_{5/2}$ $J=4$ perturber character is clearly visible. The presence of $J=2$ features is discussed in Sec. III C 1.

10(b)–10(c) show calculated $4fnf$ J spectra in excitation from various $5d_{3/2}21f$ intermediate states. The experimental excitation spectrum from $5d_{3/2}21f_{7/2}$ $J=4$, also shown in Fig. 3(b), is given in Fig. 10(a) for comparison ($4fnf$ $J=6$ is not excited from this intermediate state). In Fig. 10 the energy positions of perturbing states are indicated. The $7p_{1/2}n''f$ and $4f_{7/2}n'f$ $J=4$ perturbing states clearly affect the detected signal strength. Figure 7(a) shows a typical "shake-up–shake-down" spectrum as observed from $5d_{3/2}40f$. In this case the transition to $4f40f$ was clearly saturated. Saturation effects were included in the calculation of the oscillator-strength distribution of Figs. 7(b)–7(d), using the ICE approximation [26].

In the next section we will discuss in some detail the various $4fnf$ J series, their assignments and analyses. Some 240 observed resonances were included in the analyses. It will be shown that the $4fn'f$ spectra for $n'=8$–46 in excitation from $5dnf$ $J=5$ for $n'=13$–46

from $5dnf$ $J=4$ and for $n'=20-25$ from $J=3$ can be explained satisfactorily and that most details could be accounted for using MQDT analyses. Only five resonances, of which three are indicated in Fig. 4, remain unexplained. The identification of some 20 resonances assigned to the series discussed in Sec. III C 1 is still ambiguous.

C. $4fn'f$ series excited from $5d_{3/2}nf$ states

1. $4fn'f$ $J=2,3(,4)$ series

$4fn'f$ $J=2$ series may be excited from $5d_{3/2}nf$ $J=3,2$ states via $\Delta J=-1,0$ transitions, whereas $J=3$ series can be reached from $5d_{3/2}nf$ $J=4,3$ ($\Delta J=-1,0$). Resonances tentatively assigned as $4fn'f$ $J=2$ and/or 3 were observed in excitation spectra from $5d_{3/2}nf$ $J=3$ ($n=20-25$) and $5d_{3/2}nf$ $J=4$ ($n=13-34$).

Excitation spectra of $4fn'f$ states from $5d_{3/2}nf$ $J=3$ for $n=21$ and 20 are shown in Figs. 3(c) and Figs. 4(c) and 4(d), respectively. The analysis of the spectra for $n=21-23$ and 25 was complicated as $5d_{3/2}nf$ $J=3$ states nearly coincide with $5d_{3/2}nf$ $J=2$, 4, or 5 states, resulting in the excitation of $4fn'f$ $J=5$ or 6 features in addition to $J=2$, 3, and 4 resonances. Furthermore, the $4f_{5/2}n'f$ series are perturbed by $7p_{1/2}9f$ and $7p_{3/2}8f$ states (see Sec. III B). In spectra taken from $5d_{3/2}nf$ $J=4$, several resonances ($n'=13$, 15, and 18) with equal (reduced) quantum defect $\delta_4=0.6$ appeared. More resonances ($n'=18$, 20, 21, and 24), excited from $5d_{3/2}nf$ $J=3$ as well as $5d_{3/2}nf_{7/2}$ $J=4$, appeared to be related to this series perturbed by a state with quantum defect $\delta_3=0.2$ ($7p_{1/2}9f$) near $n'=20$. Resonances in the region $n'=27-34$ [shake-up spectrum from $5d_{3/2}25f$ $J=3$ ($n'=27,28$) and $\Delta J=-1$ transitions from $5d_{3/2}nf$ $J=4$ ($n=27-34$)] fit in the same series assuming strong interaction with two perturbing $7p_{3/2}n''f$ states ($n''=7$ and 8) with quantum defects of $\delta_1=0.5$ and $\delta_2=0.4$. The fitted R-matrix elements between the $4f_{5/2}n'f$ series with quantum defect $\delta_4=0.6$ and the two $7p_{3/2}n''f$ series both appeared to be ~ 0.2. The presence of these interactions in combination with the limited number of observed resonances makes the quantum defect of this $4f_{5/2}n'f$ $J=3$ or 2 series rather speculative. The fact that this series is observed from $5d_{3/2}nf_{7/2}$ $J=4$ at $n=21$ and 27–31 indicates a $J=3$ assignment. A $J=2$ assignment is not excluded because the $5d_{3/2}nf_{7/2}$ $J=4$ intermediate states may coincide with $5d_{3/2}nf$ $J=2$ states, which gain oscillator strength in excitation from $5d^2\,{}^3F_3$ as a result of mixing with $5d_{5/2}n'p$ perturbers ($n'=14,15$) in this region. An enhanced probability for a $\Delta J=-1$ transition from the $5d_{3/2}nf$ $J=4$ or 3 states around $n=30$ may also be attributed to mixing with $5d_{5/2}11f$ states, from which, e.g., the $7p_{3/2}8f$ character in the wave function of $4f_{5/2}n'f$ in the region of $n'=27-34$ may be excited. The presence of the sinc function (see Sec. III B) reduces the oscillator strength only by one order of magnitude for this transition. In such a transition $\Delta J=-1$ is even favored.

A second, weakly excited $4f_{5/2}n'f$ series with quantum defect $\delta_5=0.9$ was observed in spectra taken from $5d_{3/2}nf$ $J=3$ ($n=20-25$ and $n'=21-25$), $J=4$ ($n=13-34$ and $n'=14$, 16, and 22) and $J=5$ ($n=8-29$ and $n'=14,17$). Not all possible n levels were detected. Also, no energy shifts of $4f_{5/2}n'f$ states due to interaction with $4f_{7/2}n''f$ perturbers were observed. Probably, in this case, perturber admixture is hampering the observation of resonances. It was not possible to unambiguously assign the J value of this series to be 3 or 4. Scaled values for the full widths at half maximum (FWHM) were in the order of $(n^*)^3\Gamma=0.04$ hartree for both series.

We performed two separate MQDT analyses on the data collected for the series discussed above. It was possible to reproduce the linewidths of the two $4fn'f$ series using a scaled linewidth of 0.04 hartree for the $7pn''f$ perturbers as well. We generated spectra using the results of this MQDT analysis and the knowledge on $5d_{3/2}nf$ series. Examples of such calculated spectra are shown in Figs. 10(b)–10(e) and 7(b)–7(d) for excitation from $5d_{3/2}21f_{7/2}$ states. Assignments are according to the results of the Slater-Condon fit (as given in Table V and discussed in Sec. IV). The results of the MQDT analyses are collected in Table I.

2. $4fn'f$ $J=4$ series

The $4fn'f$ $J=4$ series were most strongly excited from $5d_{3/2}nf$ $J=3$ states ($\Delta J=+1$ transitions for $n=20-25$ and $n'=19-27$), but many resonances related to excitation of $4fn'f$ $J=4$ states from $5d_{3/2}nf$ $J=4$ ($n=13-34$) and $J=5$ ($n=8-29$) were observed as well (see Figs. 4, 5, and 10). Numerous strong resonances could be related to a $4f_{5/2}n'f$ series ($n'=8-29$) with quantum defect $\delta_6=1.34$, interacting with two $4f_{7/2}n''f$ series with quantum defects $\delta_4=1.25$ and $\delta_5=1.1$, respectively, and R-matrix elements $R_{46}=0.14$ and $R_{56}=0.14$. An analysis, in which only a single perturbing $4f_{7/2}nf$ series with quantum defect $\delta_4=1.20$ and $R_{46}=0.20$ was considered proved to be slightly inferior. The signals of these $4f_{5/2}n'f$ $J=4$ resonances are strongly enhanced when $4f_{7/2}nf$ character is mixed into their wave functions. This effect is clearly visible in Figs. 7 and 10. For example, the spectrum of Fig. 7(a) shows strong $4fnf$ $J=4$ resonances at $n'=36-38$ and $n'=44-47$, whereas the $J=4$ resonances at $n'=39-43$ are much weaker. In Fig. 10(a) the $J=4$ resonance at 90 008 cm^{-1} is strongly enhanced by the $4f_{7/2}16f_{5/2}$ $J=4$ perturber. Extra gain was observed close to $7pnf$ perturbing states (see Sec. III B). We could deduce quantum defects $\delta_1=0.48$, $\delta_2=0.37$, and $\delta_3=0.20$ for two $7p_{3/2}n''f$ and one $7p_{1/2}n''f$ $J=4$ series, respectively. Information on the $7pn''f$ series with $\delta_2=0.37$ and $\delta_3=0.20$ could be deduced from the observation of changes in signal strength of $4f_{5/2}n'f$ $J=4$ resonances. Coincidences with perturbed $4f_{5/2}n'f$ $J=3$ or 2 states, which might result in erroneous identification of perturber states, were taken into account. Linewidths of this $4f_{5/2}n'f$ $J=4$ series [$(n^*)^3\Gamma\sim 0.06$ hartree] are slightly larger than those of the $J=3$ or 2 series (see Sec. III C 1). The results of a MQDT analysis of the $J=4$ series are collected in Table II [quantum defects and (tentative) assignments are given

TABLE I. Parameters for the $4fnf\ J=2$ or 3 series in (a) an eight-channel and (b) a two-channel MQDT model. The index i denotes the channel, I_i the ionization limit (in cm^{-1}), and δ_i the quantum defect. The J assignment of the $4fn'f$ series is uncertain (see Sec. III C 1). Interactions with $4f_{7/2}nf$ series were not observed. The continua are indicated as c_i.

(a)

	i	1	2	3	4	5	6	7	8
		$7p_{3/2}nf$	$7p_{3/2}nf$	$7p_{1/2}nf$	$4f_{5/2}nf$	c_1	c_2	c_3	c_4
I_i		92 046.12	92 046.12	91 424.95	90 293.49				
δ_i		0.5	0.4	0.20	0.6				
R' matrix	i	1	2	3	4	5	6	7	
1									
2		0.0							
3		0.0	0.0						
4		0.2	0.2	0.1					
5		0.3	0.0	0.0	0.0				
6		0.0	0.3	0.0	0.0	0.0			
7		0.0	0.0	0.2	0.0	0.0	0.0		
8		0.0	0.0	0.0	0.4	0.0	0.0	0.0	

(b)

	i	1	2
		$4f_{5/2}nf$	c_1
I_i		90 293.49	
δ_i		0.9	
R' matrix	i	1	
2		0.4	

TABLE II. Parameters for the $4fnf\ J=4$ series in a 12-channel MQDT model. Two $4f_{7/2}n'f$ perturbing series were included (see Sec. III C 2). The index i denotes the channel, I_i the ionization limit (in cm^{-1}), and δ_i the quantum defect. The continua are indicated as c_i.

	i	1	2	3	4	5	6	7	8	9	10	11	12
		$7p_{3/2}nf$	$7p_{3/2}nf$	$7p_{1/2}nf$	$4f_{7/2}nf$	$4f_{7/2}nf$	$4f_{5/2}nf$	c_1	c_2	c_3	c_4	c_5	c_6
I_i		92 046.12	92 046.12	91 424.95	90 518.19	90 518.19	90 293.49						
δ_i		0.48	0.37	0.20	0.25	0.09	0.34						
R' matrix	i	1	2	3	4	5	6	7	8	9	10	11	
1													
2		0.0											
3		0.0	0.0										
4		0.0	0.0	0.0									
5		0.0	0.0	0.0	0.0								
6		0.15	0.05	<0.01	0.14	0.14							
7		0.2	0.0	0.0	0.0	0.0	0.0						
8		0.0	0.2	0.0	0.0	0.0	0.0	0.0					
9		0.0	0.0	0.2	0.0	0.0	0.0	0.0	0.0				
10		0.0	0.0	0.0	0.4	0.0	0.0	0.0	0.0	0.0			
11		0.0	0.0	0.0	0.0	0.4	0.0	0.0	0.0	0.0	0.0		
12		0.0	0.0	0.0	0.0	0.0	0.4	0.0	0.0	0.0	0.0	0.0	

in Table V]. In Figs. 7(d) and 10(d) calculated $J=4$ oscillator-strength distributions for excitation from $5d_{3/2}40f$ and $5d_{3/2}21f_{7/2}$ states, respectively, are included.

3. $4fn'f$ $J=5$ series

The $4fn'f$ $J=5$ series are expected to be predominantly present in excitation spectra from $5dnf$ $J=4$ intermediate states. A series which was easily identified in spectra excited from $5d_{3/2}nf$ $J=4$ (for $n=13-34$) could be assigned as $4f_{5/2}n'f$ $J=5$ ($n'=13-32$) with $\delta_3=0.8$. Examples of excitation spectra are shown in Figs. 4(b), 5, and 10(a). The $4f_{5/2}n'f$ $J=5$ series was perturbed by a $4f_{7/2}n''f$ $J=5$ series with quantum defect $\delta_2=1.1$. This interaction has little effect on the observed signal strengths of the $4f_{5/2}n'f$ $J=5$ series. The R-matrix interaction element is $R_{23}=0.13$. We had to take into account a small energy dependency in the quantum defect of this $4f_{5/2}n'f$ $J=5$ series. Several resonances were assigned to belong to a second $4f_{5/2}n'f$ $J=5$ series with quantum defect $\delta_4\sim1.1$. This series is perturbed by a single $7p_{3/2}8f$ state with quantum defect $\delta_1=0.53$ near $n'=20$ and a large interaction element ($R_{14}=0.3$) (see Fig. 9). The same $7p_{3/2}8f$ perturbing state only weakly interacts with the $4f_{5/2}n'f$ series with $\delta_3=0.8$. However, signal enhancement due to the $7p_{3/2}8f$ state in both $4f_{5/2}n'f$ $J=5$ series appears to be small, indicating a relatively large probability of decay of $7p_{3/2}8f$ $J=5$ into $6d\epsilon l$ continua. The linewidths of the $4f_{5/2}n'f$ $J=5$ series were of the same order as those of the $J=4$ series [$(n^*)^3\Gamma\sim0.06$ hartree], whereas the linewidths of $4f_{7/2}n''f$ $J=5$ states were found to be larger [$(n^*)^3\Gamma\sim0.2$ hartree]. Again, it was possible to reproduce the spectra by using a small scaled linewidth for the $7p_{3/2}n''f$ $J=5$ perturbers [$(n^*)^3\Gamma\sim0.01$ hartree]. The results of the limited $J=5$ MQDT analysis are given in Table III (quantum defects and assignments are included in Table V). Calculated $J=5$ excitation spectra from $5d_{3/2}40f$ and $5d_{3/2}21f_{7/2}$ intermediate states, respectively, are shown in Figs. 7(c) and 10(c).

4. $4fn'f$ $J=6$ series

The two possible $4f_{7/2}n''f$ $J=6$ and the single $4f_{5/2}n'f_{7/2}$ $J=6$ series can only be excited from $5dnf$ $J=5$ intermediate states, and their assignment is unambiguous. There are no $7pn''f$ $J=6$ perturber states. The $4fn'f$ $J=6$ series are interesting as in this case the important $md\epsilon d$ continua ($m=5,6$) are not available for decay. The emitted electron has to leave the atom in a high-orbital-angular-momentum state ($l_2\geq5$). This may lead to low autoionization probabilities.

The excitation spectra from $5d_{3/2}nf$ $J=5$ ($n=13-32$) contained several resonances which were not observed in the spectra taken from $J=4$ intermediate states. Their quantum defects with respect to the $4f_{5/2}$ limit are plotted in Fig. 9. This plot shows two strongly interacting $4fn'f$ $J=6$ series. Quantum defects of 0.68 and 0.54 were deduced for the $4f_{7/2}n''f$ $J=6$ and $4f_{5/2}n'f$ series, respectively. The detection efficiency of the $4fn'f$ $J=6$ series in this experiment only depends on their branching ratios into the various continua. Detected signal strengths were smaller than the calculations of oscillator strength for $\Delta J=+1$ transitions based upon jj- or jK-coupled $4fn'f$ wave functions indicate. The probable cause is that the decay of the $4fn'f$ $J=6$ into the $6d\epsilon l$ continua is large. Selection of only high-energy electrons (>4 eV) in the detector was useful to suppress $4fn'f$ $J=5,4$ signals. The $4f_{5/2}n'f$ $J=6$ series with quantum defect $\delta_2=0.68$ appeared to be relatively broad ($\Gamma\sim0.16$), whereas the $4f_{7/2}n''f$ $J=6$ series with $\delta_1=0.54$ turned out to be narrow [$(n^*)^3\Gamma<0.005$ hartree].

Perturbing $4f_{7/2}n''f$ character produced an enhanced signal strength (factor of 3) for $4f_{5/2}n'f$ $J=6$ detection.

TABLE III. Parameters for the $4fn'f$ $J=5$ series in an eight-channel MQDT model. The index i denotes the channel, I_i the ionization limit (in cm^{-1}), δ_i the quantum defect, and $\Delta\delta_i$ its energy dependency relative to the $4f_{7/2}$ limit. The continua are indicated as c_i.

i	1	2	3	4	5	6	7	8
	$7p_{3/2}nf$	$4f_{7/2}nf$	$4f_{5/2}nf$	$4f_{5/2}nf$	c_1	c_2	c_3	c_4
I_i	92046.12	90518.19	90293.49	90293.49				
δ_i	0.52	1.1	0.8	1.1				
$\Delta\delta_i$	0.0	0.0	0.08	0.0				

R' matrix i	1	2	3	4	5	6	7
1							
2	0.0						
3	0.0	0.13					
4	0.3	0.0	0.0				
5	0.13	0.0	0.0	0.0			
6	0.0	0.6	0.0	0.0	0.0		
7	0.0	0.0	0.4	0.0	0.0	0.0	
8	0.0	0.0	0.0	0.3	0.0	0.0	0.0

TABLE IV. Parameters for the $4fn'f\ J=6$ series in a four-channel MQDT model. The index i denotes the channel, I_i the ionization limit (in cm^{-1}), and δ_i the quantum defect. The continua are indicated as c_i.

	i	1 $4f_{7/2}nf$	2 $4f_{5/2}nf$	3 c_1	4 c_2
I_i		90 518.19	90 293.49		
δ_i		0.54	0.68		
R' matrix	i	1	2	3	4
2		0.59			
3		0.05	0.0		
4		0.0	0.5	0	

In the excitation from $5d_{3/2}15f\ J=5$, the interaction of $4f_{5/2}16f$ and $4f_{7/2}13f\ J=6$ states resulted in an extremely narrow resonance with laser linewidth (see Fig. 5). The results of a limited MQDT analysis of the two $J=6$ series, each interacting with one single continuum, are given in Table IV. The fitted R-matrix element between the two series was large (0.6). Quantum defects and assignments are included in Table V. $J=6$ spectra for $n=40$ and 21 calculated with the parameters resulting from the MQDT analysis are shown in Figs. 7(b) and 10(e), respectively. Although the $4fn'f\ J=6$ series cannot be excited from $5d_{3/2}21f\ J=4$, this calculated spectrum is included in Fig. 10 to facilitate comparison with the calculations for the other J values. It serves to explain the similarity in the recorded spectra plotted in Figs. 3(a) and 3(b). The second $4f_{7/2}n''f\ J=6$ series was not observed in excitation from the $5d_{3/2}nf\ J=5$ states.

D. $4f_{5/2}n'f$ and $4f_{7/2}n''f$ series excited from $5d_{5/2}nf$ states

An advantage of excitation from the $5d_{5/2}nf$ series is the possibility to excite both the $4f_{5/2}n'f$ and $4f_{7/2}n''f$ series. However, the applicability of this excitation scheme is limited by the relatively short lifetimes of the $5d_{5/2}nf$ states. For $n=17$, 19, 20, 21, 25, and 40, spectra were taken from $5d_{5/2}nf_{7/2}\ J=4$ and for $n=25$ from $5d_{5/2}nf_{7/2}\ J=5$ intermediate states. As an example, the excitation from the $5d_{5/2}20f\ J=4$ state is shown in Fig. 6. Two series were observed from the $J=4$ intermediate states with quantum defects $\delta_1=1.25$ and $\delta_2=0.86$ and from the $J=5$ intermediate state one level of a series with $\delta_3=1.38$. Signal strengths again strongly depend on the branching ratios in the autoionization decay. The branching ratios of the $4f_{7/2}n''f$ series also affected the detection efficiency of the perturbed $4f_{5/2}n'f$ series (see, e.g., Sec. III C 2). This information helps the assignment of the $4f_{7/2}n''f$ series. No perturbation of the $4f_{7/2}n''f$ by $7pn'''f$ states was observed. As shown in Fig. 6, $4f_{5/2}n'f$ features appear close to $4f_{7/2}n''f$ resonances. $4f_{5/2}n'f$ states with quantum defect 1.3 were observed in the vicinity of the $4f_{7/2}n''f$ resonances with $\delta_1=1.25$. This $4f_{7/2}n''f$ series only slightly broadened when crossing the $4f_{5/2}$ limit and was tentatively assigned as one of the $4f_{7/2}n''f\ J=4$ series interacting with the $4f_{5/2}n'f$ series with quantum defect of 1.34. This assignment is consistent with the observed signal enhancement of the latter series (see Sec. III C 2). Also, the observed linewidth of this series $[(n^*)^3\Gamma\sim 0.06$ hartree] agrees with the analysis of the $J=4$ series. Some $4f_{5/2}n'f$ resonances with quantum defect 1.1 were observed close to the series with quantum defect $\delta_2=0.86$, assigned to be a

TABLE V. Calculated level structure of the $4fnf\ J=2-6$ multiplet states for $n=15$. The third column contains quantum defects and the fourth column energy positions derived from these quantum defects. In the fifth column values calculated with the Slater-Condon fine-structure fitting routine are given and in the last column the purity of the resulting jj-coupled wave function (in %). Energy values are in cm^{-1}. Errors are estimated values.

Assignment	J	δ_i	E_{obs} (cm^{-1})	E_{calc} (cm^{-1})	Purity (%)
$4f_{5/2}15f_{7/2}$	6	0.676	89 758.4±0.5	89 759.1	99
$4f_{7/2}15f_{5/2}$	6	0.537	89 993.6±0.5	89 992.4	86
$4f_{7/2}15f_{7/2}$	6	1.38	89 926.6±5.0	89 937.1	86
$4f_{5/2}15f_{7/2}$	5	1.1	89 726.3±1.0	89 718.7	97
$4f_{5/2}15f_{5/2}$	5	0.8	89 749.2±0.5	89 748.6	97
$4f_{7/2}15f_{7/2}$	5	1.1	89 951.0±0.5	89 952.9	90
$4f_{7/2}15f_{5/2}$	5			89 943.6	90
$4f_{5/2}15f_{5/2}$	4	1.34	89 705.6±0.5	89 706.8	99
$4f_{5/2}15f_{7/2}$	4			89 720.0	99
$4f_{7/2}15f_{5/2}$	4	1.25	89 937.8±2.0	89 937.2	54
$4f_{7/2}15f_{7/2}$	4	1.1	89 951.0±2.0	89 951.8	54
$4f_{5/2}15f_{5/2}$	3			89 725.9	73
$4f_{5/2}15f_{7/2}$	3	0.9	89 741.5±2.0	89 738.0	73
$4f_{7/2}15f_{7/2}$	3	0.86	89 969.3±2.0	89 972.0	81
$4f_{7/2}15f_{5/2}$	3			89 955.9	81
$4f_{5/2}15f_{7/2}$	2	0.6	89 766.5±5.0	89 774.7	70

$4f_{7/2}n''f_{7/2}$ $J=4$ or 3. The value of ~ 1.1 for the quantum defects of this $4f_{5/2}n'f$ series would favor an assignment of $4f_{7/2}n''f_{7/2}$ $J=3$ interacting with $4f_{5/2}n'f_{5/2}$ $J=3$, according to the results of the Slater-Condon fit to be discussed in Sec. IV. However, this is rather speculative as in excitation from $5d_{5/2}nf$ only perturbed $4f_{5/2}n'f$ resonances were observed. The level with quantum defect $\delta_3=1.38$ may belong to a $4f_{7/2}n''f$ $J=6$ series, although it also might be a member of a $4f_{7/2}n''f$ $J=5$ or 4 series perturbed by a $7pnl$ state. Scaled linewidths of all observed $4f_{7/2}n''f$ resonances were 0.06 hartree.

IV. DISCUSSION

To investigate the validity of the tentative assignments discussed in Sec. III, a fitting procedure based upon a Slater-Condon analysis, using the relevant orders of direct and exchange electrostatic integrals of both f electrons, was executed. Although the number of relevant terms in the case of the $4fnf$ multiplet seems large (radial Slater integrals F^k and G^k with $k=0$, 2, 4, and 6, spin-orbit interaction parameters ζ_{4f} and ζ_{nf}), the restrictions for a correct fit are quite severe. ζ_{4f} is fixed at the value of the spin-orbit constant of the ion (64.2 cm^{-1}). The first step was to derive "unperturbed" energy values for a fictitious multiplet at $n=15$ from the quantum defects of the $4fnf$ series as obtained in MQDT analyses (Tables I–IV). This is possible because the MQDT formalism of Cooke and Cromer provides eigenquantum defects for series in the absence of channel interactions [25]. Initially, we only used those series of which the J value was unambiguously assigned ($J=6$ and 4) and only F^0, F^2, and G^0 were fitted. Based upon the outcome of this first fit, assignments were further checked by including additional series in the next steps, thus deriving values for F^4, G^2, and ζ_{nf}. Finally, the series which could not be assigned were included and all parameters fitted. Correct values for Slater integrals should comply with the constraints that $F^0>F^2>F^4>F^6>0$ and $G^0>G^2/5>G^4/9>G^6/13>0$ [27]. Furthermore, the resulting mixed wave functions must be consistent with observed oscillator strengths. As F^4, G^4, F^6, and G^6 appeared to be small, F^6 and G^6 were put to zero in the final fit.

To eliminate the mod 1 ambiguity of quantum defects, it is necessary to relate energies within the series to its lowest members, i.e., to the $4f^2$ configuration. This configuration is yet unknown, although we tried to localize it in a preliminary experiment. However, in experiments on nf series in elements having (partially) filled $4f^{14}$ shells (Yb,Au,Ra), quantum defects of ~ 1.0 have been observed [14,28]. The nf series in Ba^+ have quantum defects of ~ 0.9 [14]. We tried combinations of quantum defects between 0.0 and 1.5 in the Slater-Condon fit.

In Table V the "experimental" level energies for the fictitious $n=15$ multiplet as well as rms errors are given. These errors are induced either by strong-series perturbations (see Sec. III C 2) or reflect that only a few states of a specific series were observed (see, e.g., Sec. III D). Table V also provides level energies which result from the Slater-Condon fit. The set of electrostatic parameters F^k and G^k is given in Table VI. The errors in this table are derived from the covariance matrix resulting from the Levenberg-Marquardt minimization routine, which was used to fit the data.

TABLE VI. Values (in cm^{-1}) for Slater F^k and G^k integrals representing the fine structure of the $4f15f$ multiplet $J=2$–6. F^6 and G^6 were set to zero. F^4, G^4, and ζ_{15f} turned out to be zero within the error bars. ζ_{4f} was set to the value for the spin-orbit constant of the ion, 64.2 cm^{-1}. Errors correspond to one standard deviation.

Integral	Value
F^0	551±8
F^2	210±60
G^0	2±8
G^2	110±80

The outcome of the fit is a widely spread $4fnf$ multiplet with quantum defects between 0.0 ($J=0$) and 1.36 ($J=4$). Of the 12 levels included, 8 are reproduced satisfactorily. In the fit eventually seven parameters were used. Only F^0, F^2, and G^2 have significant values. G^0 has a value close to zero with a large error. The covariance matrix indicated a correlation between G^2 and the parameters ζ_{15f} and F^2 (and F^4). The effect of a smaller G^2 value could to a large extent be compensated by increased values for ζ_{15f} and F^2 (and F^4). This, together with the large error in G^2, accounts for the fact that G^0 appears to be smaller than G^2. Values for the parameters ζ_{15f}, F^4, and G^4 were zero within their error bounds and are not included in Table VI.

The $4f_{5/2}n'f$ $J=3,2$ series with quantum defects 0.6 did not fit well into the calculations. The series with quantum defect 0.9 may be tentatively assigned to be $4f_{5/2}n'f_{7/2}$ $J=3$ (see Sec. III C 1). Two $4f_{7/2}nf$ series (quantum defects 0.88 and 1.25, respectively) were observed in the excitation from $5d_{5/2}nf_{7/2}$ $J=4$ intermediate states (see Sec. III D). The first (0.88) may be assigned $4f_{7/2}n''f_{7/2}$ $J=3$. The assignment of the second series (1.25) remains ambiguous. It can be identified as either $4f_{7/2}n''f_{7/2}$ $J=4$ or $4f_{7/2}n''f_{7/2}$ $J=5$.

The averaged scaled FWHM linewidth $(n^*)^3\Gamma$ for the $4fnf$ configurations studied was 0.05 hartree. This is substantially below values of linewidths recently reported for the $6pnf$ series [10], although more continua are available for the decay of $4fnf$. In fact, it is comparable with the narrowest linewidths reported for the $4fng$ series ($n>7$) [7]. This appears to be different from the trend in the $6pnl$ series, where the autoionization rate decreases logarithmically for $l_2 \geq 3$ [2,10,29].

V. CONCLUSIONS

The $4fnf$ $J=5,4,3$ series from $n=46$ down to $n=8$ and the $4fnf$ $J=6$ series down to $n=13$ were studied. For n down to 10, the spectra could be explained successfully within the MQDT formalism. It turned out that it was not necessary to include a large number of interacting channels or large energy dependencies. The results of

a limited Slater-Condon analysis were used to give tentative assignments of the $4fnf$ series. The observed level splitting could be reproduced with fitted values for F^0, F^2, G^0, and G^2, although it must be emphasized that for the determination of more accurate values for the Slater integrals energies for the unknown $4fnf$ $J=0-2,7$ states have to be included in the analysis. Strong configuration interactions between $4f_{5/2}nf$ and $4f_{7/2}n'f$ series and between $4fnf$ series and low-n'' members of the $7pn''f$ series were observed, making the assignment of the $4fnf$ resonances in between $n=8$ and 10 less reliable. The number of interacting configurations rapidly increases for series converging to higher ionic states of barium. This will probably limit the applicability of MQDT to analyze autoionizing Rydberg series at energies above 11 eV.

The $4fnf$ series appear to have large quantum defects compared to other $Nlnf$ series [2,8–10,18,19,30]. This indicates large two-electron correlations.

In a preliminary experiment, we have tried to excite the $4fnf$ series for $n<8$ from the bound $5d4f$ $J=5$ states, using 200–240-nm light. So far, we did not succeed in observing these low-n $4fnf$ states. Further experiments on their excitation are being pursued in our laboratory.

Noted added in proof. During the course of the reviewing process of this paper we learned about *ab initio* eigenchannel R-matrix calculations of the $4fnf$ states in barium by Luc-Koenig and Aymar. The data points for $4fnf$ $J=6$ states, as displayed in Fig. 9, were reproduced in the calculation. Data points of $4fnf$ $J=5$ were also found in agreement, although the character of the perturber (see Fig. 8) was assigned as a second $4fnf$ $J=5$ channel, and not as a $7pnf$ $J=5$ channel.

ACKNOWLEDGMENTS

The authors wish to thank Robert Jones for making available quantum defects for the $5dnf$ $J=3$ states and Jacques Bouma for his assistance during the experiments. They gratefully acknowledge financial support from the Foundation for Fundamental Research of Matter (FOM) and the Netherlands organization for the Advancement of Research (NWO).

[1] R. Kachru, H. B. van Linden van den Heuvel, and T. F. Gallagher, Phys. Rev. A **31**, 700 (1985).
[2] R. R. Jones and T. F. Gallagher, Phys. Rev. A **38**, 2846 (1988).
[3] R. J. de Graaff, W. Ubachs, W. Hogervorst, and M. Abutaleb, Phys. Rev. A **42**, 5473 (1990).
[4] P. Camus, T. F. Gallagher, J. M. Lecompte, P. Pillet, L. Pruvost, and J. Boulmer, Phys. Rev. Lett. **62**, 2365 (1989).
[5] U. Eichman, V. Lange, and W. Sandner, Phys. Rev. Lett. **64**, 274 (1990).
[6] N. Morita and T. Suzuki, Phys. Rev. A **41**, 2370 (1990).
[7] R. R. Jones, Ph.D. thesis, University of Virginia, Charlottesville, VA (1990).
[8] R. J. de Graaff, E. A. J. M. Bente, W. Hogervorst, and A. Wannstrom, Phys. Rev. A **37**, 4532 (1988).
[9] E. A. J. M. Bente and W. Hogervorst, J. Phys. B **22**, 2679 (1989).
[10] M. Abutaleb, R. J. de Graaff, W. Ubachs, and W. Hogervorst, Phys. Rev. A **44**, 4187 (1991).
[11] E. A. J. M. Bente and W. Hogervorst, J. Phys. B **23**, 1403 (1990).
[12] J. P. Connerade, K. Dietz, M. W. D. Mansfield, and W. Weymans, J. Phys. B **17**, 1211 (1984).
[13] J. P. Connerade, Contemp. Phys. **19**, 415 (1978).
[14] C. E. Moore, *Atomic Energy Levels,* Natl. Bur. Stand. Ref. Data Ser., Natl. Bur. Stand. (U.S. GPO, Washington, DC 1971), Vol. III.
[15] F. H. Read, J. Phys. B **10**, 449 (1977).
[16] Wannier, Phys. Rev. **90**, 817 (1953).
[17] J. M. Rost and J. S. Briggs, J. Phys. B **22**, 3587 (1989).
[18] R. R. Jones (private communication).
[19] B. Carre, P. d'Oliveira, P. R. Fournier F. Gounand, and M. Aymar, Phys. Rev. A **42**, 6545 (1990).
[20] M. Abutaleb, R. J. de Graaff, W. Ubachs, W. Hogervorst, and M. Aymar, J. Phys. B **24**, 3565 (1991).
[21] R. J. de Graaff, W. Ubachs, and W. Hogervorst (unpublished).
[22] W. E. Cooke, T. F. Gallagher, S. A. Edelstein, and R. M. Hill, Phys. Rev. Lett. **40**, 178 (1978).
[23] M. Aymar, J. Phys. B **22**, 2359 (1989).
[24] A. Guisti-Suzor and H. Lefebvre-Brion, Phys. Rev. A **30**, 3057 (1984).
[25] W. E. Cooke and C. L. Cromer, Phys. Rev. A **32**, 2725 (1985).
[26] S. A. Bhatti, C. L. Cromer, and W. E. Cooke, Phys. Rev. A **24**, 161 (1981).
[27] R. D. Cowan, *The Theory of Atomic Structure and Spectra* (University of California Press, Berkeley, 1981).
[28] W. C. Martin, R. Zalubas, and L. Hagan, *Atomic Energy Levels, The Rare-Earth Elements,* Natl. Bur. Stand. Ref. Data Ser., Natl. Bur. Stand. (U.S.) Circ. No. 60 (U.S. GPO, Washington, DC, 1978).
[29] M. Poirier, Phys. Rev. A **38**, 3484 (1988).
[30] B. H. Post, W. Vassen, W. Hogervorst, M. Aymar, and O. Robeaux, J. Phys. B **18**, 187 (1985).